DEVELOPING A DESERTIFICATION ASSESSMENT SYSTEM USING A PHOTOSYNTHESIS MODEL WITH ASIMILLATED MULTI SATELLITE DATA

D. Kaneko [a, *], P. Yang [b], N. B. Chang [c], T. Kumakura [d]

[a]Remote Sensing Environmental Monitor, Inc., 4-5-5, Kamariya-nishi, Kanazawaku, Yokohama, Kanagawa, JAPAN 236-0046;
[b]Key Loboratory of Resources Remote Sensing & Digital Agriculture (Ministry of Agriculture); Institute of Agricultural Resources & Regional Planning, Chinese Academy of Agricultural Sciences, 12, Zhongguancun South Street, Haidian District, Beijing, P. R. CHINA 100081;
[c] Department of Civil, Environmental and Construction Engineering, University of Central Florida, 4000 Central Florida Blvd.Orlando, Florida, USA 32816-2450
[d]Department of Civil and Environmental Engineering, Nagaoka University of Technology, 1603-1, Kamitomioka, Nagaoka, Niigata, JAPAN 940-2188

Commission VIII, WG VIII/6

KEY WORDS: Desertification, Monitoring, Environmental modeling, Photosynthesis, Remote sensing, FLUXNET

ABSTRACT:

This paper aims to present an integrated approach for assessing the desertification processes on one hand and spot possible source locations of dust storm in Eurasian continent across the central Asia and northern China on the other hand. The authors have built Remote Sensing Environmental Monitor (RSEM) for Desertification Assessment System (DAS). Such an integrated sensing, monitoring and modeling system consists of three subsystems taking into account photosynthesis rate (PSN) based on vegetation types, water stress conditions based on the meteorological re-analysis data, and land-use/land-cover classification based on vegetation index. Eextracted normalized difference vegetation index (NDVI) anomaly helps identify the possible locations of severe dust storms linking daily photosynthesis rate with observed desertification trend in northern China with the aid of multi-sensor satellite data. To ensure the firm linkage, daily photosynthesis rate calculated were calibrated and validated by the observed tower data collected by FLUXNET at the global scale. The PSN model tends to overestimate the peak photosynthesis rate a little bit in our case study. Nevertheless, such a practice clearly confirms that land degradation in the areas from northwestern Mongolia to Mu Us desert in the Loess Plateau, and to eastern part of Inner Mongolia Autonomous Region remains the same in the past decade creating several hot spots of source locations of dust storms.

1. INTRODUCTION

At the global scale, the semi-arid belt from Spain and Tunisia in northern Sahara to the eastern end of Eurasia has been turning drier from the Roman period to the present. This dry belt in the northern hemisphere itself can be explained by the Hadley Circulation in the middle latitude zone and the Himalayan topographical effects resulting in varying precipitation trend associated with the Asian monsoon. Hence, there is an inherent linkage between the global hydrological regime, desertification, and vegetation cover. Yang et al. (2005, 2007) discussed some causal effects based on the distribution of arid areas in northern China via desert classification. The expansion of desert through the identifiable desertification processes implies that there are internal mechanisms and external forcings at both regional and global scales driving to expand the arid-belt of the Eurasian middle latitude zone. Because of the global warming impact, internal mechanisms might be due to the changes of precipitation patterns in these semi-arid or arid areas while external forcings may be mainly associated with human perturbations via economic development. All of these ended up more frequent dust storm with both extent and multitude over time, however, resulting in air pollution and public health issues. Zhang (2008) showed connected mosaic of plural Moderate Resolution Imaging Spectroradiometer (MODIS) Terra images which caught the transportation of dust particles propagating in upper atmosphere. These images showed that plumes with high dust concentrations spread to Japan and Taiwan from the northern areas of China and Mongolia. To address such integrative effects between internal mechanisms and external forcings collectively, this study aims to present a new approach by combining sensing, monitoring, and modeling efforts in one thrust to address the desertification phenomena in the middle latitude zone of these Eurasian areas. This thrust coincides with the Chinese government's National Action Programme to Combat Desertification, which deals with the same issues. In the previous studies, it is known that part of the desertification impacts were driven by human population growth as evidenced by the increase of farmland in the arid area of Shangdu County in Inner Mongolia, China (Zhao et al., 2002). These resulted in the decrease of grasslands. However, they reported there was no arid region facing land degradation or desertification in China. Wang et al. (2007) classified deserts into three phases in regard to how low level these areas could be in terms of sustainable land use when they were cultivated as crop land. For this reason, they proposed possible conservation

* Corresponding author.

policies via afforestation to replace the crop land in these arid areas. Of the Eurasian continent, the upper part of the middle latitude zone includes important boreal forests of Taiga having positive effects of CO_2 sequestration. In contrast, the southern part of the middle latitude zone has potential of land degradation. This motivates the enlargement of our study region to cover broader type of land use allowing us to consider the desertification processes from boreal forested areas (Taiga) to shrub land, to savanna, to herbaceous grasslands, and to sand dunes or vise versa. No matter which route could occur, it is simply the result of rising air temperature and changing precipitation rates and variances on one hand and land-use and land-cover changes due to human perturbations on the other hand. During the past two decades, interactions between human perturbations such as expanding agricultural activities to feed ever increasing population and the changes of natural environments due to global warming are particularly salient in northern China. We therefore proposed an integrated sensing, monitoring and modeling system that consists of three subsystems taking into account photosynthesis rate (PSN) based on vegetation types, water stress conditions based on the meteorological re-analysis data, and land-use and land-cover classification based on vegetation index. Our hypothesis can thus be defined as that when the seasonal transitions move on, the source locations of dust storms may be identified in spring over every year with such a desertification assessment system (DAS), which is a component of Remote Sensing Environmental Monitor (RSEM) system for crop production, grassland, forest and environmental mitigation for Megapolises using the concept of vegetation and photosynthesis. It is anticipated that DAS will lead us to generate a suite of better conservation plans or policies as to the afforestation endeavor in these arid areas and ultimately mitigate environmental and social impacts on these capital cities of Beijing, Soul, and Tokyo due to periodic dust storm events.

2. LITERATURE REVIEW

Three approaches for desertification research in the Eurasian long band of arid lands are worth mentioning. The first approach is to develop numerical simulation models from the viewpoints of climate change impacts and seasonal anomalies of dry meteorological conditions (Nakajima et al., 2004). Such models may simulate the sources of dust storms from which storms happened to roll up on past dust events in eastern Asia (Nakajima et al., 2004; Tanaka and Chiba, 2005). Such a study compared the simulated areas of high sand flux with the observed sites of the dust storm appearance. The source of sand emission from the arid grounds was Taklimakan Desert and Kupqi and Tengger Deserts due to strong wind erosion in northern China. The second approach is to monitor the desertification processes using satellite remote sensing (Piao et al, 2005, Huang and Siegert, 2006).

In this type of application, land classification in arid regions with the aide of extracting high potential areas of desertification was carried out based on the NDVI derived from SPOT VEGETATION in China. The third approach is to develop

combined method using both modeling and remote sensing. In this type of application, satellite-based Normalized Difference Vegetation Index (NDVI) analysis with wild fire concern using an autoregressive AR(1) model was carried out (Hill et al., 2008). They characterized vegetation dynamics using NDVI estimates from the coarse scale, hyper-temporal 1-km MEDOKADS archive, which is based on calibrated NOAA–AVHRR images. We promote the third approach to build up the DAS using process-based photosynthesis model in this study field.

3. MATERIALS AND METHODS

This study shows the actual land degradation trend in relation to the Eurasian desertification. Focus has been placed on proving that the desertification is developing in these regions from Takli Makan desert to Inner Mongolia Autonomous Region. Two computed land degradation assessment tools that play a critical role in the integrated assessment include the anomaly of NDVI and the changing PSN distribution in grassland areas. The values of NDVI were derived based on the SPOT VEGETATION images and the PSN rates were estimated and using MODIS data. The basic expression of the photosynthesis rate for the grasslands is expressed as follows (Kaneko et al., 2009).

$$PSN = f_{rad} \cdot f_{Syn}(T_c) \cdot \beta_s \cdot eLAI \tag{1}$$

$$f_{rad\_PC} = \frac{1}{2m} \cdot \{a \cdot PAR + PSN_{\max}\} - \frac{1}{2m} \cdot \sqrt{(a \cdot PAR + PSN_{\max})^2 - 4m \cdot a \cdot PSN_{\max} PAR} \tag{1a}$$

in which PSN signifies the photosynthesis rate ($gCO_2/m^2/day$), PAR denotes the photosynthetically active radiation (MJ/m^2), β_s is the stomatal opening (no dimension), T_c represents the canopy temperature (°C), eLAI stands for the effective leaf area index (no dimension), a is the Prioul–Chartier constant (no dimension), PSN_{max} represents the maximum PSN ($gCO_2/m^2/day$), and c_c is the curve convexity constant (dimensionless). The stomata β_s is expressed using the Crop Water Stress Index (CWSI), which is defined as the ratio of actual evapotranspiration (E_{ac}) divided by the Penman potential evaporation (E_p). The values of E_{ac} and E_p are supplied from NCMWF to compute horizontal distributions of the PSN. We also applied a complementary model to monitor paddy yields at Japanese sites and in Nanjing, China using meteorological data for the evaluation of accuracy of E_{ac} and E_p provided by NCMWF. The temperature response function of the photosynthesis rate f_{Syn} is such that the rate PSN falls at low air temperatures. The function f_{Syn} shows an S-shaped curve defined by Eq. (2), which is well known as the sigmoidal logistic type function

$$f_{Syn}(T_c) = \left[\frac{1}{1 + \exp\{k_{syn}(T_c - T_{hv})\}} \right], \tag{2}$$

where T_{hv} is the temperature parameter at half of the maximum photosynthesis rate (°C), and k_{syn} is the gradient constant of the relation between the function $f_{Syn}(T_c)$ and the canopy temperature, which is approximated by the air temperature at 2 m above the ground surface. The temperature response functions for low-temperature sterility and high-temperature injury are defined as the following equations, referring to curves reported by Vong and Murata (1997).

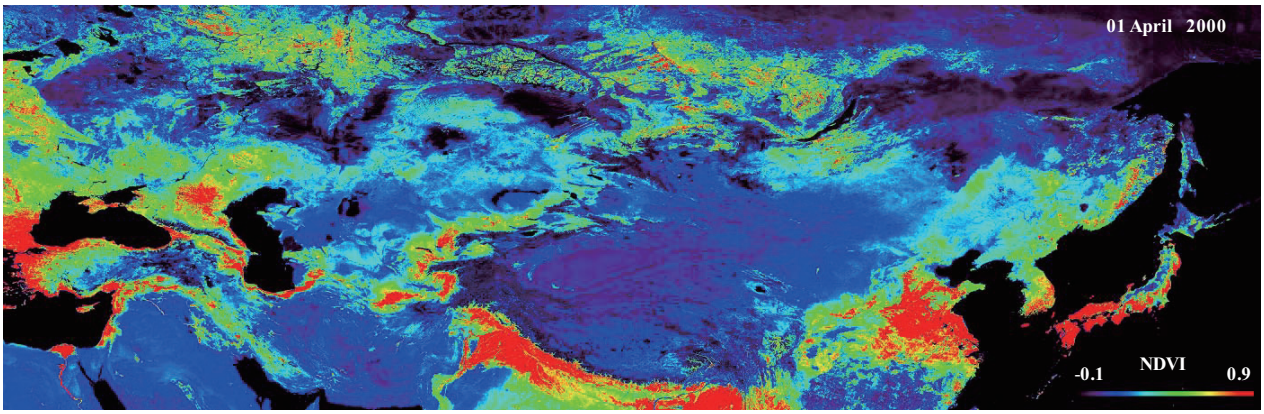

Figure 1. Horizontal distribution of NDVI derived from SPOT VEGETATION in Eurasian arid areas distributed in middle latitude zone (1-10, April 2001)

$$f_{Lster}(T_c) = 1 - \exp\left[k_{Lster}\left(T_{Lster} - T_c\right)\right] \quad (3a)$$

$$f_{Hster}(T_c) = 1 - \exp\left[k_{Hster}\left(T_c - T_{Hster}\right)\right], \quad (3b)$$

In those equations, k_{Lster} is the low-temperature sterility constant, T_{Lster} is the low-sterility limit temperature (°C), k_{Hster} is the high-temperature injury constant, T_{Hster} is the high-injury limit temperature (°C), and T_c is the plant leaf temperature (°C).

Finally, the response function of the compounded temperature sterility affects both low-temperature and high-temperature injury in grain production. It is expressed as shown below.

$$F_{Ster}(T_s) = f_{Lster}(Tc) \cdot f_{Hster}(T_c) \quad (4)$$

4. DATA COLLECTION, ANALYSIS, AND SYNTHESIS

The sharp decrease of NDVI distribution in grasslands implies the deterioration of land in association with desertification. Within this context, NDVI data were extracted with 1km resolution SPOT VEGETATION images taking the grassy level into account for desertification assessment. Table 1 summarizes the episodes of dust storms which were detected by Japanese dust storm observation network. Bold character in Table 1 represents the time windows that dust storms occurred in Beijing. The time windows of those episodes were used for

year	City	China	Japan & China			China	Remark
		Yinchuan	Beijing (bold)			Shnaghai	
	Analysis		March	April	May		
1993					5/5		severest
2000	◎	4/4,4/8	3/10, 3/12	4/6, 4/9			heavy
2001			3/19, 20, 21				
			3/17, 18	4/9, 10, 11, 12,			
2002			3/20	13,14,15			heavy
2003			3/27	4/13, 14			
2004			3,11,12	4/21, 22			
				4/21, 22,			
2005				4/14, 15, 16			
2006	○			4/16, 17			
				4/24,25,4/8	4/30,5/1		
2007	○		3/27, 28	4/1, 2, 3	5/26, 27	39540	severest
2008			3/3, 4				

Table 1. Observation days of dense dust particles transported to Japan

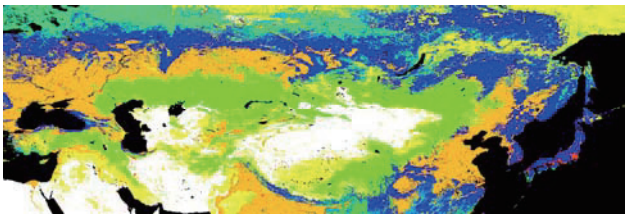

Figure 2. Land cover distribution extracted from MODIS data. Desert is white, bare land is yellow, and grassland is light green, while forest is blue and cropland is ochre

computing NDVI anomalies to extract the source locations of dust storms in northern China and Mongolia. We calculated the mean NDVI during 2000-2008 years. The cloud cover sometimes affects considerably on the calculation of NDVI especially in the grass growth season. Consequently, 10 days of Max Value Composite (MVC) was adopted for the assessment in this arid area to avoid cloud cover effects. Figure 1 shows a snapshot of horizontal distribution of NDVI in April, 2000 when the propagation of severe dust storm occurred in eastern Asia. The dense vegetation belt of grain plants in the southern part of the Eurasia is presented with the red color. On the other hand, the grassland areas with small NDVI in early spring are shown with light blue. The grassy areas of central Asia are lineated by light green though.

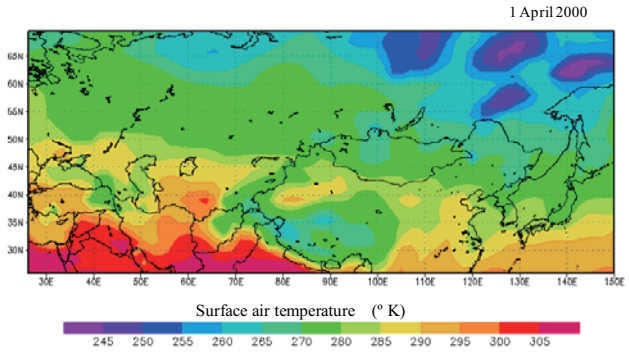

Figure 3. Distributions of surface air temperature on 1 April in Eurasian middle latitude zone

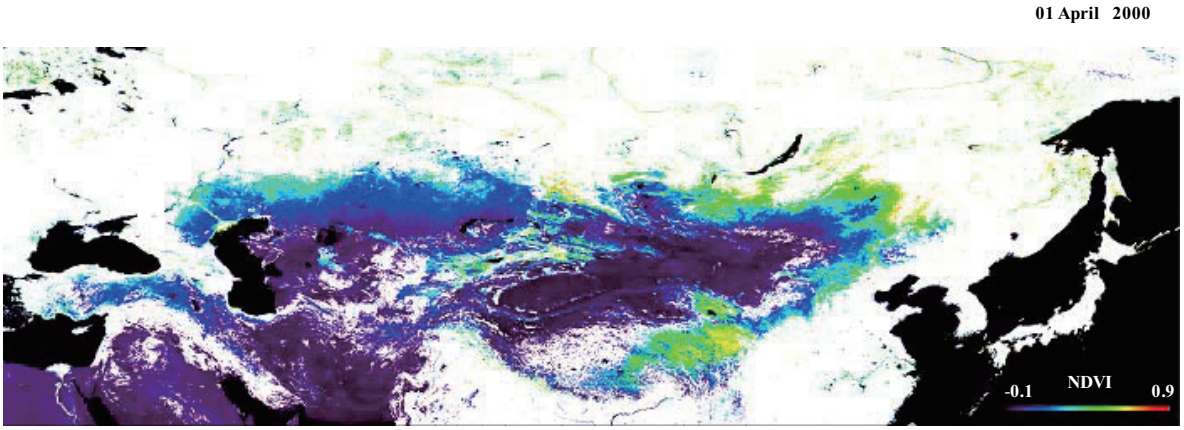

Figure 4. Distribution of NDVI in grassland and desert spread over Eurasian middle latitude zone

MODIS images offer fundamental land cover classification across the globe. We extracted the distribution of the grassland, desert, crop land, and forest areas in the Eurasian continent, as shown in Figure 2. The grassy plains and deserts were the dominant types of land cover in this region. What is of particular interest is to take into consideration of the effects of surface air temperature rise because of global warming and the anthropogenic expansion of northern regions to be the potential crop cultivation areas. The latter concern requires the assessment of boreal forests in Siberia where the PSN rates need to be produced with the aid of NDVI and meteorological re-analysis data. Figure 3 thus displays a distribution of surface air temperature adopted from the National Centers for Environmental Prediction (NCEP). The surface air temperature distribution was used for computing the temperature response function of the PSN in Asia.

5. MODEL CALIBRATION

We compared the computed values of our model with worldwide data reported by Falge et al. (2002) to assure the model integrity. The collected data are the ground observation results that cover worldwide FLUXNET data at 35 tower sites. The largest gross primary productivity (GPP) was 14.4 ($\mu molCO_2m^{-2}s^{-1}$) and the biggest ecosystem respiration (RE) equaled 6.6 ($\mu molCO_2m^{-2}s^{-1}$) at Little Washita in U.S.A. This observation site associated with AmeriFlux is situated in a tall grassy plain in the state of Oklahoma. Similarly, the greatest GPP was 39.2 ($\mu molCO_2m^{-2}s^{-1}$) and RE was 15.0 ($\mu molCO_2m^{-2}s^{-1}$) at Shidler in the same state of Oklahoma of a tall grassy plain. Annual net ecosystem productivity (NEP) was -212 ($gCm^{-2}year^{-1}$) at Little Washita, while NEP was 362 ($gCm^{-2}year^{-1}$) at Shilser. Another NEP was 538 ($gCm^{-2}year^{-1}$) at Risoe in Denmark by EUROFLUX (now renamed as CarboEurope). Daily average values of NEP were 2.13 ($gCm^{-2}year^{-1}$) at Risoe and 2.26 ($gCm^{-2}year^{-1}$) at Shilder, respectively. According to the report by Falge et al. (2002), NEP per day shared a small value of 20.2% in GPP at the grassy plain. The observational evidence suggests that one of the reasons is the release of large carbon accumulated in the underground. On the other hand, Falge et al. (2002) reported that net primary productivity (NPP) produced only by vegetation in the grassland ranges from 40% to 80% of GPP.

With this said in the US and Europe, the largest PSN rates was 20 ($gCO_2m^{-2}day^{-1}$) at the Asian grassy plains in the summer based on the present model. This value means that the converted PSN rate in terms of CO_2 becomes a big value of 5.5 ($gCO_2m^{-2}day^{-1}$) by using the molecular weight ratio of C/CO_2 (0.273). Li et al. (2005) reposted that the peak daily sums of NEE, GEP, and total ecosystem respiration (Reco) were - 2.3, 3.5, 1.5 ($gCm^{-2}day^{-1}$), respectively, in the grassy plains which were sparse dry grassland in Mongolia. Gross ecosystem productivity (GEP) was 3.5 in the same grassland at Kherlenbayan Ulaan in Mongolia. It can be concluded that the night respiration in this model is half of the daily respiration which occupies 35% of GPP. We calculated the NPP by deducting night respiration from NPP that was 5.5. The peak result of NPP was 85.7% given that the GPP was 5.5, i.e., the value of 4.7 ($gCm^{-2}day^{-1}$) is the calculated maximum NPP using this model. According to the observations at the same spot of Mongolia done by Mariko et al. (2007), CO_2 flux of the soil at dry grassland was 75~250 (mg $CO_2m^{-2}h^{-1}$). The estimated daily soil emission thus becomes about 1~2 ($gCO_2m^{-2}day^{-1}$) indicating that it shared only less than 10% of the largest PSN (20 $gCO_2m^{-2}day^{-1}$) in daytime in Asia based on our photosynthesis model. When eddy covariance method adopted by FluxNet tends to underestimate around 20% of PSN (Wilson, 2002), the PSN rate in the daytime of this study becomes 4.2 approximately 20 percent surcharges for 3.5 ($gCm^{-2}day^{-1}$). It is therefore confirmed that the calculated value of the PSN using our model is reasonable, but the model tends to overestimate

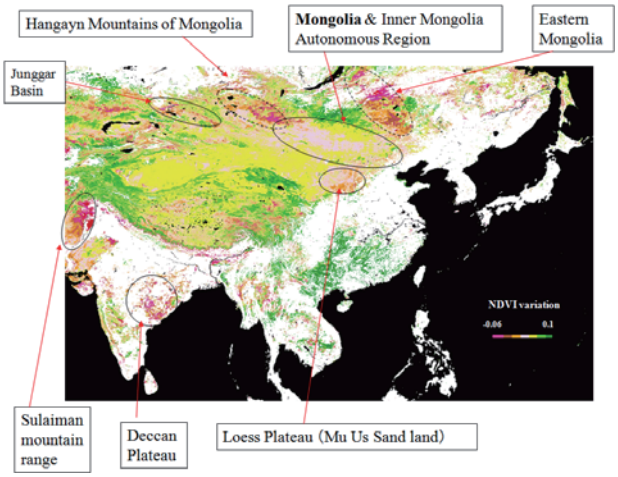

Figure 5. Distribution of computed photosynthesis rate in grassland in Asia on 1 August, 2001

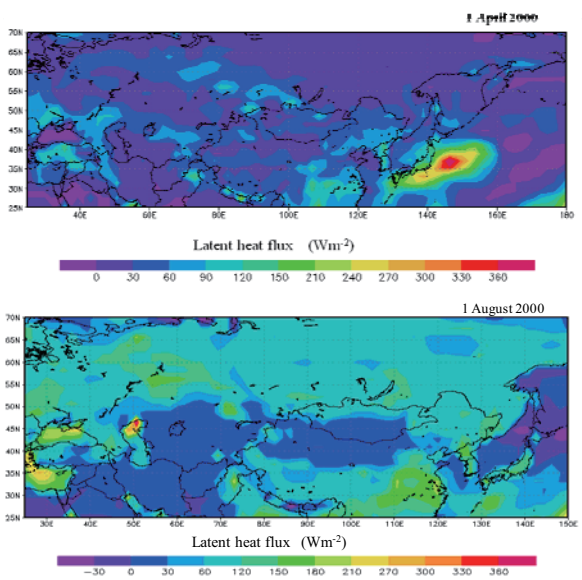

Figure 6. Distributions of latent heat flux in Eurasian areas

PSN around 10%. However, the computed value could overestimate the maximum PSN. Because the observed values must be small as the grassland at Kherlenbayan Ulaan is sparse. The largest GPP of the grassy plain was thus obtained by multiplying a factor of 1.143 relative to PSN calculated. The results GPP_{max} is equal to 6.3 ($gCm^{-2}day^{-1}$). The observed daily mean GPP values were 10.72 and 6.30 ($gCm^{-2}day^{-1}$) over a tall prairie at Shilder and Little Washita in Oklahoma (Falge et al., 2002). The ratio 4.4/6.3 equals 0.698 which indicates that the value of NPP can be estimated as 4.4 that is about 70% of the GPP (=6.3). This value implies that the computed maximum PSN is a little bigger in a range from 40% to 80% of GPP, whose percents were shown by Falge et al. (2002). Despite the coincident of the computed value with that at Little Washita data in the middle value of three calibration sites, the maximum GPP must be larger by considering the effect of the average in growing season. The author should discuss further the calibration using other Asian data, since the observed values distribute in the wide range of GPP which depends on geological sites and types of grassland plants.

6. RESULTS AND DISCUSSION

Within this study, the years that had dust storm episodes were selected and all the degraded areas due to desertification in the study region were extracted based on the annual variations of NDVI distributions. It is assumed that the distribution of mean values of NDVI follows the normal distribution. The deviation of NDVI from its calculated mean was used as the evidence of land degradation from which the source of impacts can be more salient with respect to the desert and grassland areas extracted based on these values of NDVI as shown in Figure 1 and land cover data based on MODIS as shown in Figure 2.

Figure 4 presents the distribution of extracted NDVI on 1-10 August, 2000. Broad grassy plains expressed by light green color spread over Kazakhstan along northern areas of Caspian sea, Mongolia's south of Baycal lake, and Qinghai province in China. Dense grassland scatters in Inner Mongolia Autonomous Region and the mountainous areas of Qinghai province. The grassy level at the northern parts of the Taklimakan exhibits the sparse patterns in the areas of the Kazakhstan eastern prairie.

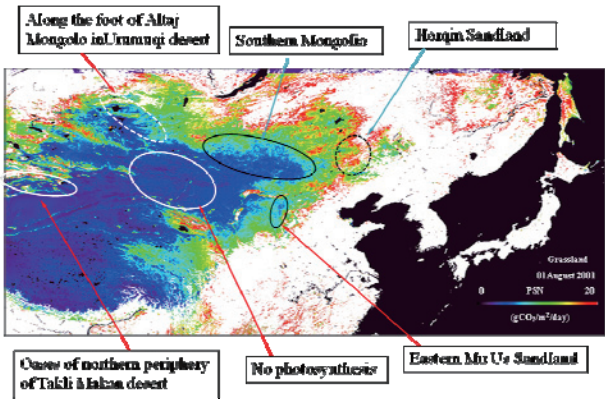

Figure 7. Relation between degraded desertification areas and the photosynthesis rate

The region with sharp drop of NDVI implies degradation especially in the Mu Us desert. Figure 4 also presents the fact that desertification processes were in fast progress in the Mongolia northwest areas and the eastern edge of Mongolia. This was further confirmed by Yoshino (1997) indicating that the frequency of the dust storm occurrence was high in the neighborhood of the border of China and Mongolia. Yang et al. (2005) reported that wind erosion was the greatest factor of the desertification, and was particularly severe in such arid regions of western Taklimakan Desert, southern areas of oasis' along Tarim river, Turpan basin, Junggar basin, southern areas of Gobi Desert, the Badain Jaran Desert, and Tengel Desert situated in western areas of the Yinchuan city. According to Zhang et al. (2008), the dust particles that were rolled up in Taklimakan desert could go north into the Mongolia areas. MODIS images showed that northwestern winds transported the yellow dust clouds to Japan.

When there are no internal mechanisms and external forcings of desertification, the changes of vegetation cover at the semi-arid areas would mainly be driven by seasonal variations of air temperature and precipitation over years. It has yet been answered by that either internal mechanisms or external forcings on a long-term basis could be more important. The photosynthesis rates were computed using the equation (1) over the dust storm areas in northern China and Mongolia. Yang et al. (2005) expressed the desertification processes in terms of three classes associated with the levels of wind erosion. We also compared the PSN rates against the desert distributions reported by Zhao et al. (2002) and Yang (2005). In addition, the distribution of the PSN rates were compared with the horizontal spreads of vegetation anomalies that were extracted from the deviation of NDVI based on the annually-averaged NDVIav. The grassland areas with a declined trend were shown in Figure 5 in red color. Those degraded areas were mainly in the proximity along the Sulaiman mountain range which is situated in the western (right) river bank of the Indus middle basin, and the southern region of Hangayn Mountains of Mongolia, the border zone of two countries between the Lake Baikal in Russia, and in eastern areas of Mongolia. In addition to these areas, Figure 5 suggests that the desertification processes was in progress in the wide range of Mongolia and the border region of Inner Mongolia Autonomous Region, and the Mu Us desert of the Loess Plateau. These arid areas were originally sparse in vegetation and the slight decrease of NDVI could mean the high possibility of land degradation caused by either internal mechanisms or external forcings or both.

Figure 6 depicts the distributions of latent heat flux derived from CNES data in Eurasia. The areas with small values from 25 to 30 (Wm^{-2}) spread horizontally from Taklimakan desert to eastern Mongolia. These areas were dry and sparsely vegetated. Figure 7 shows an example of PSN rate distribution computed by the proposed model according to the above equations. These areas expressed by the colors from sky-blue to light green confirm the photosynthetic rates were still considerable. Even if the desertification processes were phenomenal, it confirms that the grassy level was still abundant. This characteristics turns out to be different with the observational evidence derived from the anomalies based on the mean NDVI. On the other hand, the desert areas with poor vegetation were shown by black color in Figure 6, where photosynthetic rates were approximately zero. This suggests that the values of NDVI in grassy lands were dropped quickly facing substantial decline of vegetation cover.

7. CONCLUSIONS

This study aims to present a holistic assessment of desertification and source locations of dust storm in the Eurasian continent. Our RSEM system for DAS enables us to assess the evolution of grassy plains distributed over the middle latitude zone out of the Eurasia. This DAS system is designed based on the synergistic potential of sensing, monitoring and modeling by assimilating vegetation index and land cover derived from multi satellite sensors along with meteorological re-analysis data. The model calibration using FLUXNET indicated that the estimated PSN results in our study areas are reasonable but the present model tends to overestimate a little the peak photosynthesis rate in Asian continent. The extracted time series of the NDVI anomalies help pin down the source location of severe dust storm over years. Modeling outputs allow us to compare the results of daily photosynthesis rate with the observed desertification trends being previously reported in northern China. It is observed that the desertification processes are in fast progress in the areas from northwestern Mongolia to Mu Us desert of the Loess Plateau and eastern part of Inner Mongolia Autonomous Region. The right bank of the middle basin along Indus River in Pakistan appears to be another hot spot.

REFERENCES

Falge, E., Baldocchi, D., Tenhunen, J., Aubinet, M., Bakwin, P., Berbigier, P., Bernhofer, C., Burba, G., Clement, R., Kenneth J., Davis, Elbers, J. A., Goldstein, A. H., Grelle, A., Granier, A., Guðmundsson, J., Hollinger, D., Kowalski, A.S., Katul, G., Law, B. E., Malhi, Y., et al., 2002. Seasonality of ecosystem respiration and gross primary production as derived from FLUXNET measurements. *Agricultural and Forest Meteorology*, Vol. 113, Issues 1-4, 2, pp. 53-74.

Huang, S. and Siegert, F., 2006. Landcover classification optimized to detect areas at risk of desertification in North China based on SPOT VEGETATION imagery, *Journal of Arid Environment.* Vol. 67, pp. 308-327.

Kaneko, D., Kumakura, T., Yang, P., 2009. Data assimilation for crop yield and CO_2 fixation monitoring in Asia by a photosynthetic-sterility model using satellites and meteorological data. *International Journal of Global Warming* Vol. 1(3), pp. 179-200.

Jingzhu Zhao, Gan Wu, Hongmei Kong, Yingmin Zao, Guofan Shao, Qi Lu, 2002. Strategies to combat desertification for the twenty-first century in China. *Int. J. Sustain. Dev. World Ecol.* Vol. 9, pp. 292-297.

Li, D. S.-G., Asanuma, J., Eugster, W., Kotani, A., Liu, J.,-J., Urano, T., Oikawa, T., Davaa, G., Oyunbaatar, D., and Sugita M., 2005. Net ecosystem carbon dioxide exchange over grazed steppe in central Mongolia. *Global Change Biology*, Vol. 11 (11), pp. 1941 – 1955.

Mariko, S., Urano, T., and Asanuma, J., 2007. The Rangelands Atmosphere-hydrosphere-biosphere Interaction Study Experiment in Northeastern Asia (RAISE). *Journal of Hydrology*, Vol. 333, 1, pp. 118-123.

Mukai, M., T. Nakajima, and T. Takemura, 2004. A study of the long-term trend of mineral dust aerosol distributions in Asia using a general circulation model. *J. Geophys. Res.*, Atmospheres, Vol. 109, D19204, pp. 19.

Piao, S., Fang, J., Liu, H., Zhu, B., 2005. NDVI-indicated decline in desertification in China in the past two decades. *Geophysical Research Letters*, Vol. 32, L06402 pp. 4.

Tanaka, T. Y., and M. Chiba, 2005. Global simulation of dust aerosol with a chemical transport model, MASINGAR, *J. Met. Soc. Japan*, Vol. 83A, pp. 255-278.

Vong, N. Q., Murata, Y., 1997. Studies on the physiological characteristics of C3 and C4 crop species. I. The effects of air temperature on the apparent photosynthesis, dark respiration and nutrient absorption of some crops. *Japanese J. of Crop Science* Vol. 46, pp. 45-52.

Wilson, K., Goldstein, A., Falge,E., Aubinet, M, Baldocchi, D., Berbigier, P., Bernhofer, C., Ceulemans, R., Dolman, H., Field, C., Grelle, A., Ibrom, A., Law, B.E., Kowalski, A., Meyers, T., Moncrieff, J., Monson, R., Oechel, W., Tenhunen, J., Valentini, R., et al., 2002. Energy balance closure at FLUXNET sites, *Agricultural and Forest Meteorology*, Vol. 113, Issues 1-4, Vol. 2, pp. 223-243.

Yang, X., Ding, Z., Fan, X., Zhou, Z., Ma, N., 2007. Processes and mechanisms of desertification in northern China during the last 30 years, with a special reference to the Hunshandake Sandy Land, eastern Inner Mongolia, *Catena,* Vol. 71, pp. 2-12.

Yang, X., Jia, B., Ci, L., Zhang, K., 2005. Desertification assessment in China: An overview. *J. of Arid Environments,* Vol. 63, pp. 517-531.

Zhang, W.L., Chen, S.P., Chen, J., Wei, L., Han, X.G., Lin, G.H., 2007. Biophysical regulations of carbon fluxes of a steppe and a cultivated cropland in semiarid Inner Mongolia. *Agricultural and Forest Meteorology*, Vol. 146, Issues 3-4, pp. 216-229.

ACKNOWLEDGMENTS

This study is funded by a Grant-in-Aid (No. 21580319) for Scientific Research. We wish to express thanks to the Japan Society for the Promotion of Science, of the Ministry of Education, Culture, Sports, Science and Technology. We aim to supply freely the fundamental information products from this monitoring system for world societies with the concepts of NPO and the Global Earth Observation System of Systems (GEOSS).